

First-principles study of heat transport properties of graphene nanoribbons

Zhen Wah Tan,^{†,‡} Jian-Sheng Wang,[¶] and Chee Kwan Gan^{*,‡}

*Department of Physics, Cornell University, 109 Clark Hall, Ithaca, New York 14853-2501,
U.S.A., Institute of High Performance Computing, 1 Fusionopolis Way, #16-16 Connexis,
Singapore 138632, Singapore, and Center for Computational Science and Engineering, and
Department of Physics, National University of Singapore, Singapore 117542*

E-mail: ganck@ihpc.a-star.edu.sg

Abstract

We use density-functional theory and the nonequilibrium Green's function method, as well as phonon dispersion calculations to study the thermal conductance of graphene nanoribbons with armchair and zigzag edges, with and without hydrogen passivation. We find that low-frequency phonon bands of the zigzag ribbons are more dispersive than those of the armchair ribbons, and that this difference accounts for the anisotropy in the thermal conductance of graphene nanoribbons. Comparing our results with data on large-area graphene, edge effects are shown to contribute to thermal conductance, enhance the anisotropy in thermal conductance of graphene nanoribbons, and increase thermal conductance per unit width. The edges with and without hydrogen-passivation modify the atomic structure and ultimately influence the phonon thermal transport differently for the two ribbon types.

*To whom correspondence should be addressed

[†]Cornell University

[‡]Institute of High Performance Computing

[¶]National University of Singapore

Keywords: Graphene nanoribbons, thermal transport, nonequilibrium Green's function, phonon dispersion

Introduction

Graphene nanoribbons (GNR), or strips of planar graphene,¹ exhibit several novel properties such as large magnetoresistance² and high electron mobility³ which prove to be useful in nanoscale electronics. Graphene is known to have extremely high thermal conductivity⁴ that depends on the flake size⁵ and number of atomic planes.⁶ GNR are expected to retain good thermal properties. This, together with the availability of simpler fabrication techniques than carbon nanotubes,⁷ has caused GNR to gain much attention in recent years due to their potential applications in modern devices. Experimental and theoretical work have concluded that GNR can be metallic or semiconducting,^{8–10} and the energy gap varies with ribbon width^{8,11,12} and edge orientation.⁹ These properties make semiconducting GNR an attractive alternative channel material¹³ capable of producing smaller devices than those achievable with silicon. Metallic GNR can also be used as interconnects,¹⁴ and having circuits made entirely of GNR holds the possibility of reducing or eliminating contact resistance.¹⁵ For these reasons, various methods for fabricating GNR have been developed,^{10,16,17} including scanning tunneling microscope lithography that offers precise control of the structure of ribbons.¹⁸ Recent developments have also enabled the production of sub-10-nanometer GNR,¹⁹ and greater control over edge geometries.²⁰ Prototype GNR field-effect transistors have also been developed and characterized.^{21,22}

While the electronic properties of GNR have been explored in depth, thermal transport in GNR—an important consideration for thermoelectric performance and thermal management—has also gained more attention recently.^{23–26} Several studies have been made on the phonon dispersions^{27–30} of GNR, while more recent articles have focused on phonon-mediated thermal transport³¹ of GNR. For example, Sevinçli and Cuniberti have investigated the thermoelectric performance of edge-disordered GNR.³² Hu *et al.*²⁴ observed that ZGNR have higher thermal conduc-

tance than AGNR of comparable widths, and attributed this to different phonon scattering rates intrinsic to the ribbon geometry. Several other studies have also confirmed the anisotropy in thermal conductance of GNR,^{33,34} and a similar anisotropy has been predicted by Jiang *et al.*³⁵ in graphene. In this Letter, we employ density-functional theory (DFT) that accurately deals with the atomic and electronic structures, the nonequilibrium Green function method that has been shown to be useful in studying the electron³⁶ and heat transport through nanostructures,³⁷ and also the standard theory of lattice dynamics to account for phonon transport through GNR. We investigate how the atomic structures of GNR affect the phonon dispersions and ultimately thermal transport, and explain the anisotropy in thermal conductance of GNR.

Methodology

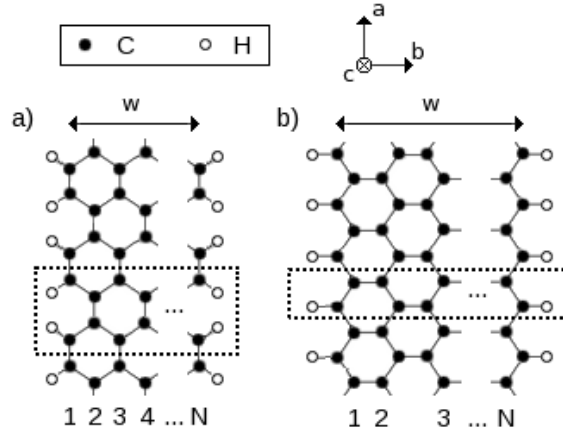


Figure 1: Hydrogen-passivated graphene nanoribbons with (a) armchair edges (AGNR- N), and (b) zigzag edges (ZGNR- N). A primitive unit cell is marked out in each case, and the ribbons are periodic in the a -direction. The number N denotes the number of C atoms in the b -direction, and the ribbon width W is given by the maximal distance between C atoms in the b -direction.

Because systems of sub-nanometer widths will become important with the miniaturization of GNR-based devices, we study the thermal conductance in narrow, pristine GNR by combining first-principles density-functional calculations and the ballistic nonequilibrium Green's function (NEGF) method.^{37,38} In this work, we investigate the thermal conductance of armchair GNR (AGNR- N) of widths $N = 3, 4, 5, 6$ (refer to [figure][1][1a for the meaning of N), as well as

zigzag GNR (ZGNR- N) of widths $N = 2, 3, 4, 5$ (Figure 1b). We obtain the force-constant matrix via DFT calculations implemented in SIESTA.³⁹ We use periodic boundary conditions on the orthorhombic supercell consisting of nine primitive unit cells: The ribbons are periodic in the a -direction (see Figure 1), and each ribbon is separated from its nearest neighbors by 16 Å of vacuum in the b - and c -directions. To facilitate NEGF calculations, we partition the supercell into three blocks with three primitive unit cells per block. These three blocks are for the central junction, the left and right lead regions as described in Ref.³⁸ We note that the same force constants required for NEGF calculations can be readily used to calculate the phonon dispersion curves.

For DFT calculations, the local-density approximation with the exchange-correlation functional due to Perdew and Zunger is used. We use a rather fine mesh cutoff of 400 Ry. As demonstrated by Son *et al.*⁹ and Gan *et al.*,⁴⁰ spin-polarization effects are particularly important in ZGNR, therefore we use spin-polarized calculations for ZGNR in this work. Nonspin-polarized calculations are used for AGNR.

We first perform ionic relaxation of GNR using a conjugate-gradient method. To obtain the best possible relaxed structure while ensuring that the conjugate-gradient minimization converges, we use a force tolerance of 0.001 eV/Å. To construct a force-constant matrix, we sequentially displace each atom from its equilibrium position in the a -, b - and c -directions by a distance of 0.015 Å, and evaluate the forces acting on all atoms as a result of each displacement.⁴¹ A central finite difference scheme is used to evaluate the force-constant matrix, which is required by the NEGF and the phonon calculations.

Using the ballistic NEGF method,^{37,38} we then calculate the phonon transmission coefficient \tilde{T} for each GNR system. Thermal conductance is evaluated using the Landauer formula:

$$\sigma(T) = \int_0^\infty \frac{d\omega}{2\pi} \hbar \omega \tilde{T}(\omega) \frac{\partial f}{\partial T}, \quad (1)$$

where the occupation distribution function $f(\omega, T) = 1/(e^{\hbar\omega/k_B T} - 1)$. It is important to note that ?? implies that at low temperatures, low-frequency modes are the dominant factor in thermal

transport since the derivative $\partial f/\partial T$ diminishes rapidly with increasing ω .

We find the thermal conductance of GNR to be independent of ribbon length in the ballistic regime, as noted previously by Lan *et al.*³¹ This is consistent with the theory of ballistic transport based on the Landauer formula, where diffusive behaviors cannot be addressed. The ballistic assumption is valid for small systems, such as the ones studied in this work, where the system size is much smaller than the graphene phonon mean free path of ~ 775 nm at room temperature.⁵ However, in the case of large-area graphene, diffusive (Umklapp-limited) scattering plays a significant role in reducing thermal conductivity, as determined theoretically⁴² and experimentally.^{43,44}

Results

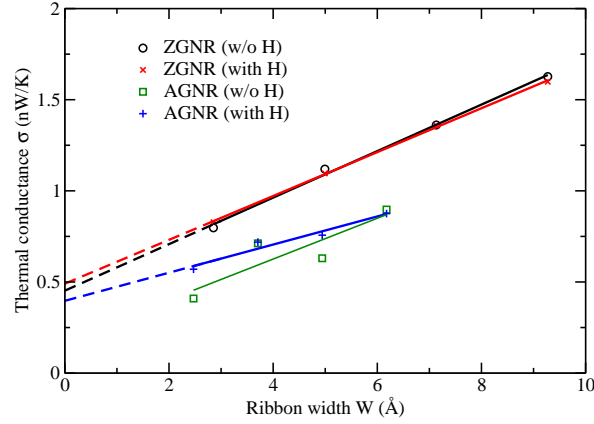


Figure 2: (color online) Thermal conductance σ (at 300 K) of GNR as a function of ribbon width W , for ZGNR- N with $N = 2, 3, 4, 5$ and AGNR- N with $N = 3, 4, 5, 6$. Data shown are for ZGNR without H-passivation, ZGNR with H-passivation; AGNR without H-passivation, and AGNR with H-passivation—linear fits have correlation coefficients 0.998, 1.000, 0.882 and 0.978, respectively. Gradients of the linear fits are 1.276, 1.203, 1.119 and 0.771 W/(m K), while vertical intercepts are 0.4523, 0.4906, 0.178 and 0.3967 nW/K, respectively.

[figure][2][2] shows the thermal conductance (at 300 K) of various GNR as a function of ribbon width W . In the limit of large width, the conductance of a ribbon is proportional to its width, and our data exhibit a similar trend: For ZGNR with and without H-passivation, and for AGNR with H-passivation, the thermal conductance increases linearly with width, with high correlation coefficients of 0.978 and above. While thermal conductance of AGNR without H-passivation generally increases with temperature, it does not follow a strictly linear trend. On the other hand, on

extrapolating the linear trends to $W = 0$ Å, we see positive contributions to the thermal conductance (~ 0.5 nW/K) that stem from edge effects. This is consistent with the findings by Xu *et al.*,³³ which show a sharp increase in thermal conductance per unit width as W decreases from 1 nm to 0.5 nm, where edge effects becomes more evident. [figure][2][2] also shows that ZGNR generally have higher conductance than AGNR of comparable widths. The main reason for this is due to the larger transmission coefficients $\tilde{T}(\nu)$ for the ZGNR compared to AGNR of comparable widths, as shown in [figure][3][3]. This observation is explained in the following paragraphs.

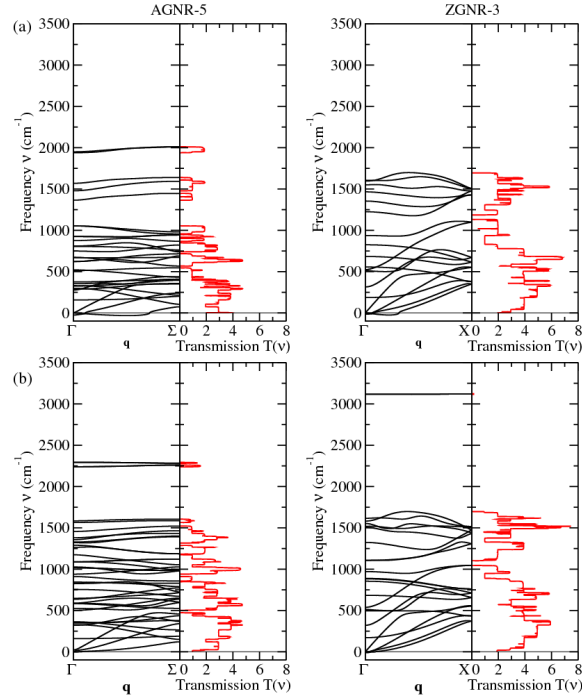


Figure 3: (color online) Comparison between phonon dispersions (left panel) and transmission coefficients (right panel) for AGNR-5 and ZGNR-3, (a) without and (b) with H-passivation. Imaginary-frequency modes are indicated by $\nu < 0$ cm⁻¹. The two ribbons have comparable widths: $W_{\text{AGNR-5}} = 4.942$ Å, $W_{\text{ZGNR-3}} = 4.993$ Å.

According to the NEGF formalism for 1D systems,^{45–47} the transmission coefficient $\tilde{T}(\nu)$ is the number of phonon modes at any frequency $\nu = \omega/2\pi$. This can be readily seen in [figure][3][3], where we compare the phonon dispersions with the transmission coefficient for AGNR-5 and ZGNR-3, with and without H-passivation. We see that $\tilde{T}(\nu)$ essentially equals to the number of bands at frequency ν , except at very low frequencies. We expect that the discrepancy at low frequencies between $\tilde{T}(\nu)$ from NEGF calculations and that deduced from phonon bands is caused

by intricate differences in the numerical treatments for these two methods. For example, in our NEGF calculation, it is assumed that two atoms cease to interact with one another (i.e., the force constant between them is set to zero) once they are separated by more than three primitive cells. However, we do not truncate force-constant matrix elements in the phonon calculations. The slightly imaginary modes near Γ from the phonon calculations suggest that the GNR is unstable with respect to long wavelength periodic distortion, a fact that is consistent with the compressive edge stresses that are inherent in the GNR edges.⁴⁰ Despite small numerical uncertainties for extremely low frequency modes (which may be eliminated by adopting a larger supercell at the expense of incurring larger computational costs), the data obtained for $\tilde{T}(\nu)$ is sufficiently accurate for conductance calculations. Since $\tilde{T}(\nu)$ is equal to the number of phonon modes present, dispersive phonon bands would generally lead to larger values of $\tilde{T}(\nu)$ than less dispersive bands.

The dispersion relations in [figure][3][3] indicate that low-frequency phonon bands in ZGNR-3 tend to be more dispersive than those in AGNR-5. The ribbons have comparable widths, with $W_{\text{ZGNR-3}} = 4.993 \text{ \AA}$, and $W_{\text{AGNR-5}} = 4.942 \text{ \AA}$. The dispersive bands in ZGNR-3 would give rise to higher $\tilde{T}(\nu)$ in the low-frequency regime: low-frequency modes play a dominant role in thermal conductance at room temperature. Thus, the fact that low-frequency bands in ZGNR-3 are more dispersive than those in AGNR-5 explains the anisotropy in thermal conductance, even in the ballistic limit.

Since the transmission coefficients are intimately related to the phonon dispersions, we have systematically studied the phonon dispersion of the ribbons of different width and orientations (i.e., AGNR- N and ZGNR- N), with and without hydrogen passivation, where the results are summarized in [figure][4][4]. The dispersion trends, cut-off frequencies, and C-H stretching mode frequencies agree very well with previously published data calculated using REBOII and MO/8 simulations.^{29,30} Also, DFT calculations by Gillen *et al.*²⁸ yielded very similar phonon dispersion trends for ZGNR, with cut-off frequencies of $\sim 1650 \text{ cm}^{-1}$, and C-H stretching mode frequencies of $\sim 3100 \text{ cm}^{-1}$, while we obtain $\sim 1700 \text{ cm}^{-1}$ and $\sim 3120 \text{ cm}^{-1}$ respectively.

It is interesting to note that in most of the test cases, the lowest phonon modes are found to

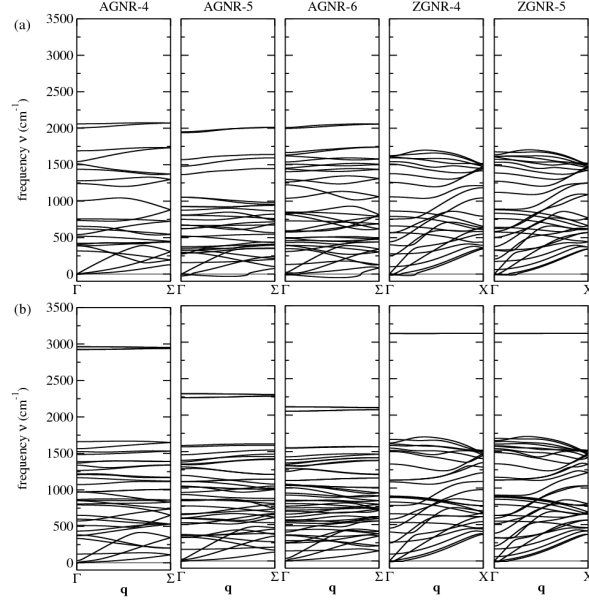


Figure 4: Phonon dispersion plots for AGNR-4, 5, 6 and ZGNR-4, 5 (a) without H-passivation and (b) with H-passivation. Imaginary frequencies are indicated by $\nu < 0 \text{ cm}^{-1}$.

soften and have imaginary frequencies—an indication of instability—near Γ . These imaginary-frequency modes (denoted by $\nu < 0 \text{ cm}^{-1}$) are shown in [figure][4][4]. The lowest modes are edge waves with out-of-plane displacements, and the unstable edge rippling generally occurs over a range of about 10% the Brillouin zone size, corresponding to wavelengths larger than 2 nm (4 nm) for ZGNR (AGNR). This result is consistent with a study by Shenoy *et al.*,⁴⁸ which indicates that GNR form edge ripples with wavelengths of about 8 nm due to edge stresses.

The phonon plots in [figure][4][4] show that in general, ZGNR have low-frequency bands that are more dispersive than those in AGNR. The reasoning for ZGNR-3 having higher thermal conductance than AGNR-5 can thus be applied also to relate the anisotropic behavior of GNR: More dispersive low-frequency bands in ZGNR result in larger transmission coefficients $\tilde{T}(\nu)$ as compared to AGNR in the low-frequency regime, thereby giving rise to higher thermal conductance in ZGNR.

A similar anisotropy in thermal conductance in graphene sheets has been pointed out by Jiang *et al.*,³⁵ using the valence force field model. The study found a thermal conductance per unit width, $\sigma/W = 0.348$ and 0.352 W/(m K) in the armchair and zigzag directions, respectively. Similar find-

ings have been obtained by Hu *et al.*²⁴ and Guo *et al.*²³ through molecular dynamics simulations for GNR with larger N . Hu *et al.* attributed the difference in thermal conductance between AGNR and ZGNR to the presence of different phonon scattering mechanisms. However, since we observe that the anisotropy persists in the ballistic regime, we suggest that the anisotropy in thermal conductance could also be due to the anisotropy in phonon dispersion for GNR.

On the other hand, the fitted gradients of our σ versus W plots for H-passivated ribbons are 0.771 and 1.203 W/(m K), respectively. This suggests that edge effects increase the σ/W ratio, and magnify the anisotropy in thermal conductance for GNR. These trends indicate that arrays of narrow ZGNR may be most efficient in thermal management, whereas wide AGNR may optimize thermoelectric performance of graphene-based transistors, with its lower thermal conductance.

Table 1: Thermal conductance data of GNR. Thermal conductance at 300 K is σ , in units of nW/K. The conductance shift due to H-passivation is $\Delta = (\sigma_{\text{withH}} - \sigma_{\text{w/oH}})/\sigma_{\text{w/oH}}$.

N	AGNR			ZGNR		
	$\sigma_{\text{w/oH}}$	σ_{withH}	Δ	$\sigma_{\text{w/oH}}$	σ_{withH}	Δ
2				0.797	0.828	3.9%
3	0.409	0.570	39.4%	1.119	1.096	-2.1%
4	0.712	0.719	1%	1.361	1.358	-0.2%
5	0.630	0.757	20.1%	1.627	1.599	-1.7%
6	0.897	0.875	-2.5%			

In considering the effects of H-passivation on σ , we define the thermal conductance shift by $\Delta = (\sigma_{\text{withH}} - \sigma_{\text{w/oH}})/\sigma_{\text{w/oH}}$. Table [table][1][1] shows that while Δ stays below 4% for ZGNR, Δ can reach as high as 39% for AGNR. This disparity can be traced to the modification of phonon modes with H-passivation.

[figure][4][4] shows that H-passivation induces little change to the dispersion relations for ZGNR, compared to AGNR. For ZGNR, despite the addition of six phonon bands (due to two extra H atoms), these bands have high frequencies ($\nu > 700 \text{ cm}^{-1}$) and thus do not contribute significantly to thermal conductance at room temperature. On the other hand, for AGNR, we see that H-passivation causes more drastic changes to phonon dispersions. Besides having twelve more phonon bands due to the four H atoms, the phonon bands also generally shift towards lower fre-

quencies. To explain the latter, we note that H-passivation reduces the strong C–C triple bonds at the armrests of AGNR^{49,50} to a much weaker edge bond. However, in ZGNR, only one in two edge C atoms have dangling bonds, thus edge C–C bonds are weaker than double bonds, and relax only slightly upon H-passivation. Bond relaxation causes a reduction in force constants and phonon frequencies, and this change takes place more significantly in AGNR than in ZGNR.

It should also be noted that for AGNR with and without H-passivation, the thermal conductance varies non-trivially with ribbon width, with larger variations observed in the cases without H-passivation. Previous studies on AGNR have shown that the variation of energy gaps^{9,49,51} and edge energies⁴⁰ with ribbon width can be grouped into three distinct families (with respect to $N \bmod 3$). However, we have been unable to verify such trends in thermal conductance for AGNR due to huge computational costs for systems of larger N .

Conclusions

We have studied phonon-mediated thermal conductance of graphene nanoribbons with armchair (AGNR) and zigzag (ZGNR) edges of sub-nanometer ribbon widths through density-functional calculations, a nonequilibrium Green’s function method, and phonon calculations. ZGNR was found to have higher thermal conductance than AGNR of comparable widths, due to an anisotropy in the phonon dispersion for GNR: low-frequency bands in ZGNR are more dispersive than those in AGNR. Edge effects were found to produce a positive contribution (~ 0.5 nW/K) to thermal conductance, increase thermal conductance per unit width, and cause ZGNR to have a significantly higher thermal conductance per unit width (~ 1.2 W/(m K)) than AGNR (~ 0.77 W/(m K)). These facts suggest that narrow ZGNR can act as good thermal conductors for thermal management, while wide AGNR may be a better candidate for application in nanoscale devices. Thermal conductance of AGNR and ZGNR change differently with hydrogen-passivation at the edges: Edge C–C bonds in AGNR are relaxed by a greater extent than those in ZGNR, thus phonon frequencies in AGNR are more significantly reduced than those in ZGNR. It remains interesting to determine if

thermal conductance in AGNR follows the same trends as that for energy gap and edge energy, as this will yield further insight on thermal transport mechanisms in AGNR. This may shed some light in understanding the thermoelectric behavior of AGNR, and ultimately be useful for applications in nanoscale electronics.

Finally, we note that the combination of density-functional theory, nonequilibrium Green's function method and phonon dispersion calculations reveal, for the first time, the peculiar heat transport properties that could be traced to the intricate interplay between the atomic structures, the transmission coefficients and the dispersiveness of the phonon bands. Our study provided a natural link between these quantities and explained the anisotropy observed in the thermal conductance of zigzag and armchair GNR.

Acknowledgments

The authors gratefully acknowledge invaluable discussions with Julian D. Gale, Jinghua Lan, Gang Wu, and Jinwu Jiang.

References

- (1) Novoselov, K. S.; Geim, A. K.; Morozov, S. V.; Jiang, D.; Zhang, Y.; Dubonos, S. V.; Grigorieva, I. V.; Firsov, A. A. *Science* **2004**, *306*, 666–669.
- (2) Kim, W. Y.; Kim, K. S. *Nature Nanotech.* **2008**, *3*, 408.
- (3) Bolotin, K. I.; Sikes, K. J.; Jiang, Z.; Kilma, M.; Fudenberg, G.; Hone, J.; Kim, P.; Stormer, H. L. *Solid State Commun.* **2008**, *146*, 351.
- (4) Balandin, A. A.; Ghosh, S.; Bao, W.; Calizo, I.; Teweldebrhan, D.; Miao, F.; Lau, C. N. *Nano Lett.* **2008**, *8*, 902.
- (5) Ghosh, S.; Calizo, I.; Teweldebrhan, D.; Pokatilov, E. P.; Nika, D. L.; Balandin, A. A.; Bao, W.; Miao, F.; Lau, C. N. *Appl. Phys. Lett.* **2008**, *92*, 151911.

- (6) Ghosh, S.; Bao, W.; Nika, D. L.; Subrina, S.; Pokatilov, E. P.; Lau, C. N.; Balandin, A. A. *Nature Materials* **2010**, 9, 555.
- (7) Barone, V.; Hod, O.; Scuseria, G. E. *Nano Lett.* **2006**, 6, 2748.
- (8) Nakada, K.; Fujita, M.; Dresselhaus, G.; Dresselhaus, M. S. *Phys. Rev. B* **1996**, 54, 17954.
- (9) Son, Y. W.; Cohen, M. L.; Louie, S. G. *Phys. Rev. Lett.* **2006**, 97, 216803.
- (10) Li, X.; Wang, X.; Zhang, L.; Lee, S.; Dai, H. *Science* **2008**, 319, 1229–1232.
- (11) Han, M. Y.; Ozyilmaz, B.; Zhang, Y.; Kim, P. *Phys. Rev. Lett.* **2007**, 98, 206805.
- (12) Chen, Z.; Lin, Y. M.; Rooks, M. J.; Avouris, P. *Physica E* **2007**, 40, 228.
- (13) Obradovic, B.; Kotlyar, R.; Heinz, F.; Matagne, P.; Rakshit, T.; Giles, M. D.; Stettler, M. A.; Nikonov, D. E. *Appl. Phys. Lett.* **2006**, 88, 142102.
- (14) Shao, Q.; Liu, G.; Teweldebrhan, D.; Balandin, A. A. *Appl. Phys. Lett.* **2008**, 92, 202108.
- (15) Naeemi, A.; Meindl, J. D. *IEEE Elect. Dev. Lett.* **2007**, 28, 428.
- (16) Yang, X.; Dou, X.; Rouhanipour, A.; Zhi, L.; Rader, H. J.; Mullen, K. *J. Am. Chem. Soc.* **2008**, 130, 4216.
- (17) Jiao, L.; Zhang, L.; Wang, X.; Diankov, G.; Dai, H. *Nature* **2009**, 458, 877.
- (18) Tapasztó, L.; Dobnik, G.; Lambin, P.; Biro, L. P. *Nature Nanotech.* **2008**, 3, 397.
- (19) Bai, J.; Duan, X.; Huang, Y. *Nano Lett.* **2009**, 9, 2083.
- (20) Cai, J.; Ruffieux, P.; Jaafar, R.; Bieri, M.; Braun, T.; Blankenburg, S.; Muoth, M.; Seitsonen, M. P.; Saleh, M.; Feng, X.; Müllen, K.; Fasel, R. *Nature Lett.* **2010**, 466, 470.
- (21) Yan, Q.; Huang, B.; Yu, J.; Zheng, F.; Zhang, J.; Wu, J.; Gu, B. L.; Liu, F.; Duan, W. *Nano Lett.* **2007**, 7, 1469.

- (22) Wang, X.; Ouyang, Y.; Li, X.; Wang, H.; Guo, J.; Dai, H. *Phys. Rev. Lett.* **2008**, *100*, 206803.
- (23) Guo, Z.; Zhang, D.; Gong, X. G. *Appl. Phys. Lett.* **2009**, *95*, 163103.
- (24) Hu, J.; Ruan, C.; Chen, Y. P. *Nano Lett.* **2009**, *9*, 2730.
- (25) Ghosh, S.; Nika, D. L.; Pokatilov, E. P.; Balandin, A. A. *New J. Phys.* **2009**, *11*, 000000.
- (26) Xu, Y.; Chen, X.; Wang, J.-S.; Gu, B.-L.; Duan, W. *Phys. Rev. B* **2010**, *81*, 195425.
- (27) Qian, J.; Allen, M. J.; Yang, Y.; Dutta, M.; Stroscio, M. A. *Superlatt. Microstruct.* **2009**, *46*, 881.
- (28) Gillen, R.; Mohr, M.; Thomsen, C.; Maultzsch, J. *Phys. Rev. B* **2009**, *80*, 155418.
- (29) Vandescuren, M.; Hermet, P.; Meunier, V.; Henrard, L.; Lambin, P. *Phys. Rev. B* **2008**, *78*, 195401.
- (30) Yamada, M.; Yamakita, Y.; Ohno, K. *Phys. Rev. B* **2008**, *77*, 054302.
- (31) Lan, J.; Wang, J.-S.; Gan, C. K.; Chin, S. K. *Phys. Rev. B* **2009**, *79*, 115401.
- (32) Sevinçli, H.; Cuniberti, G. *Phys. Rev. B* **2010**, *81*, 113401.
- (33) Xu, Y.; Chen, X.; Gu, B.-L.; Duan, W. *Appl. Phys. Lett.* **2009**, *95*, 233116.
- (34) Bi, K.; Chen, Y.; Chen, M.; Wang, Y. *Solid State Commun.* **2010**, *150*, 1321.
- (35) Jiang, J.-W.; Wang, J.-S.; Li, B. *Phys. Rev. B* **2009**, *79*, 205418.
- (36) Brandbyge, M.; Mozos, J.-L.; Ordejon, P.; Taylor, J.; Stokbro, K. *Phys. Rev. B* **2002**, *65*, 165401.
- (37) Wang, J.-S.; Wang, J.; Zeng, N. *Phys. Rev. B* **2006**, *74*, 033408.
- (38) Wang, J.-S.; Zeng, N.; Wang, J.; Gan, C. K. *Phys. Rev. E* **2007**, *75*, 061128.

- (39) Soler, J.; Artacho, E.; Gale, J. D.; García, A.; Junquera, J.; Ordejón, P.; Sánchez-Portal, D. *J. Phys.: Condens. Matter* **2002**, *14*, 2745.
- (40) Gan, C. K.; Srolovitz, D. J. *Phys. Rev. B* **2010**, *81*, 125445.
- (41) Gan, C. K.; Feng, Y. P.; Srolovitz, D. J. *Phys. Rev. B* **2006**, *73*, 235214.
- (42) Nika, D. L.; Pokatilov, E. P.; Askerov, A. S.; Balandin, A. A. *Phys. Rev. B* **2009**, *79*, 155413.
- (43) Freitag, M.; Steiner, M.; Martin, Y.; Perebeinos, V.; Chen, Z.; Tsang, J. C.; Avouris, P. *Nano Lett.* **2009**, *9*, 1883.
- (44) Nika, D. L.; Ghosh, S.; Pokatilov, E. P.; Balandin, A. A. *Appl. Phys. Lett.* **2009**, *94*, 203103.
- (45) Yamamoto, T.; Watanabe, S.; Watanabe, K. *Phys. Rev. Lett.* **2004**, *92*, 075502.
- (46) Rego, L. G. C.; Kirczenow, G. *Phys. Rev. Lett.* **1998**, *81*, 232.
- (47) Wang, J.-S.; Wang, J.; Lü, J. T. *Eur. Phys. J. B* **2007**, *98*, 206805.
- (48) Shenoy, V. B.; Reddy, C. D.; Ramasubramaniam, A.; Zhang, Y. W. *Phys. Rev. Lett.* **2008**, *101*, 245501.
- (49) Kawai, T.; Miyamoto, Y.; Sugino, O.; Koga, Y. *Phys. Rev. B* **2000**, *62*, R16349.
- (50) Koskinen, P.; Malola, S.; Hakkinen, H. *Phys. Rev. Lett.* **2008**, *101*, 115502.
- (51) Fujita, M.; Igami, M.; Nakada, K. *J. Phys. Soc. Japan* **1997**, *66*, 1864.